How to cite: *Angew. Chem. Int. Ed.* **2022,** *61,* e202200905
International Edition: doi.org/10.1002/anie.202200905
German Edition: doi.org/10.1002/ange.202200905

COF Membranes Hot Paper

Solvent-Influenced Fragmentations in Free-Standing Three-Dimensional Covalent Organic Framework Membranes for Hydrophobicity Switching

*Abdul Khayum Mohammed, Ayesha A. Al Khoori, Matthew A. Addicoat, Sabu Varghese, Israa Othman, Maguy Abi Jaoude, Kyriaki Polychronopoulou, Maria Baias, Mohammad Abu Haija, and Dinesh Shetty**

Abstract: The ordered open organic frameworks membranes are attractive candidates for flow-assisted molecular separations. The physicochemical properties of such membranes mostly depend on their selectively chosen functional building blocks. In this work, we have introduced a novel concept of functional switchability of three-dimensional covalent organic framework (3D-COF) membranes through a simple solvent-influenced fragmentation method. This room-temperature interfacial synthesis provides free-standing 3D-COF membranes with distinct physicochemical properties from the same building monomers. Notably, the change of solvent from chloroform to ethyl acetate switches the membrane property from hydrophilic (water contact angle 60°) to hydrophobic (water contact angle 142°) nature. The hydrophobic 3D-COF membrane selectively passes oil molecules from an oil–water emulsion with a gravitational flux of 1536 $L m^{-2} h^{-1}$.

[*] Dr. A. K. Mohammed, I. Othman, Prof. M. A. Jaoude, Prof. M. A. Haija, Prof. D. Shetty
Department of Chemistry, Khalifa University, Abu Dhabi (United Arab Emirates)
E-mail: dinesh.shetty@ku.ac.ae

A. A. Al Khoori, Prof. K. Polychronopoulou
Department of Mechanical Engineering, Khalifa University, Abu Dhabi (United Arab Emirates)

A. A. Al Khoori, Prof. M. A. Jaoude, Prof. K. Polychronopoulou, Prof. M. A. Haija, Prof. D. Shetty
Center for Catalysis and Separations, Khalifa University, Abu Dhabi (United Arab Emirates)

Dr. M. A. Addicoat
School of Science and Technology, Nottingham Trent University, Clifton Lane, Nottingham NG11 8NS (UK)

Dr. S. Varghese, Prof. M. Baias
Science Division, New York University, Abu Dhabi (NYUAD), Abu Dhabi (United Arab Emirates)

Introduction

Covalent organic frameworks (COFs) have been explored as tunable crystalline and porous materials for task-specific applications, including gas and energy storage, catalysis, molecular separation, and optoelectronics.[1] The two-dimensional (2D) or three-dimensional (3D) covalently connected organic molecules in COFs maintain their heterogeneous features in various solution environments. Although layered 2D-COFs are widely explored for their macroscopic features,[2] the potential utilities of 3D-COFs are still mostly limited to their native granular form.[3] The 3D bonding pattern results in interconnected open pores, enhancing the molecular diffusion through the framework matrix. Therefore, a free-standing 3D-COF membrane could be an attractive candidate for molecular separation applications. However, unlike weak pi–pi interactions between layers in 2D-COFs, the atomic organization in 3D-COF principally originated from the spatially oriented covalent bonds. As a result, it is difficult to crystallize and assemble the framework into large free-standing macroscopic structures such as membranes. The attempts to fabricate 3D-COFs into macroscopic structures are mainly limited to the mixed matrix membranes or support-based thin films,[4] limiting the full exploration of pristine structure and open porosity. Therefore, the direct fabrication of free-standing 3D-COF membranes is a highly desirable but highly challenging task to achieve.

Moreover, the functional tunability of COFs is generally limited to the strategic selection of molecular building blocks.[5] For example, controlling COF membrane properties such as hydrophobicity without altering the building block combinations or post-synthetic modifications is difficult to realize and no studies have been reported thus far. The hydrophobicity is one of the important physicochemical properties of membranes for many important applications including oil–water separation, membrane distillation, and molecular sieving.[6] In this regard, a simple and one-step facile method to tune the hydrophobicity of membrane is fundamentally attractive and highly useful for technology transfer. Recently, a reversible covalent bonding strategy has been adopted for constructing a hydrophilic-hydrophobic gradient 2D-COF thin-film membrane for distilla-

tion-based desalination of water, which shows the staggering importance of such research.[7]

In this work, we have successfully synthesized the free-standing 3D-COF membranes and introduced a novel pre-synthetically controlled framework growth strategy to tune the hydrophobicity of the resulting membranes. We developed an efficient interfacial method at room temperature to regulate the extension of defects in the imine (C=N) bonded covalent 3D-network composed of tetrakis(4-amino)phenylmethane (Tam) and 2, 5-dibromoterephtahdehyde (Dbta) (Figure 1) by changing the biphase solvent systems (ethyl acetate/water or chloroform/water). Notably, the resulting 3D-COF membranes exhibit unique physicochemical properties because of the extent of defect sites within the network structures. The ethyl acetate/water system results in in situ fragmentation of the 3D-COF membrane (Tam Dbta-1) with a higher number of free-aldehyde functional groups (HC=O) in the framework compared to the chloroform/water system where a lower number of unreacted aldehydes groups were observed (Tam Dbta-2). This chemical tuning of the framework significantly controlled the resulting membranes' properties: Tam Dbta-1 was highly hydrophobic (142°) compared to the Tam Dbta-2 (60°) due to more exposed halogen atoms in the framework fragments. Furthermore, the hydrophobic self-standing Tam Dbta-1 membrane was successfully explored for the demulsification of oil molecules from the water–oil mixture through simple gravity filtration and observed a high flux of 1536 $L m^{-2} h^{-1}$. Thus, our simple and effective method to control the functional tunability in the free-standing 3D-COF membranes would open new COF-based membrane design possibilities for desired applications.

Results and Discussion

The 3D-COF membranes were fabricated through the p-toluenesulphonic acid-catalyzed interfacial polymerization reactions (Figure 1a and b). Tam Dbta-1 and Tam Dbta-2 were synthesized at the interface of biphasic solvents; ethyl acetate: water and chloroform: water, respectively. The catalyst and all other reaction conditions were maintained the same for both imine condensation reactions. The aqueous solution (10 mL) of Tam (0.039 mmol) and the PTSA catalyst (0.15 mmol) was interfaced with organic solution (10 mL) of Dbta (0.078 mmol) at room temperature for 48 hours. The obtained thin-film membranes from these interfaces were collected and washed with hot water, hot *N*,

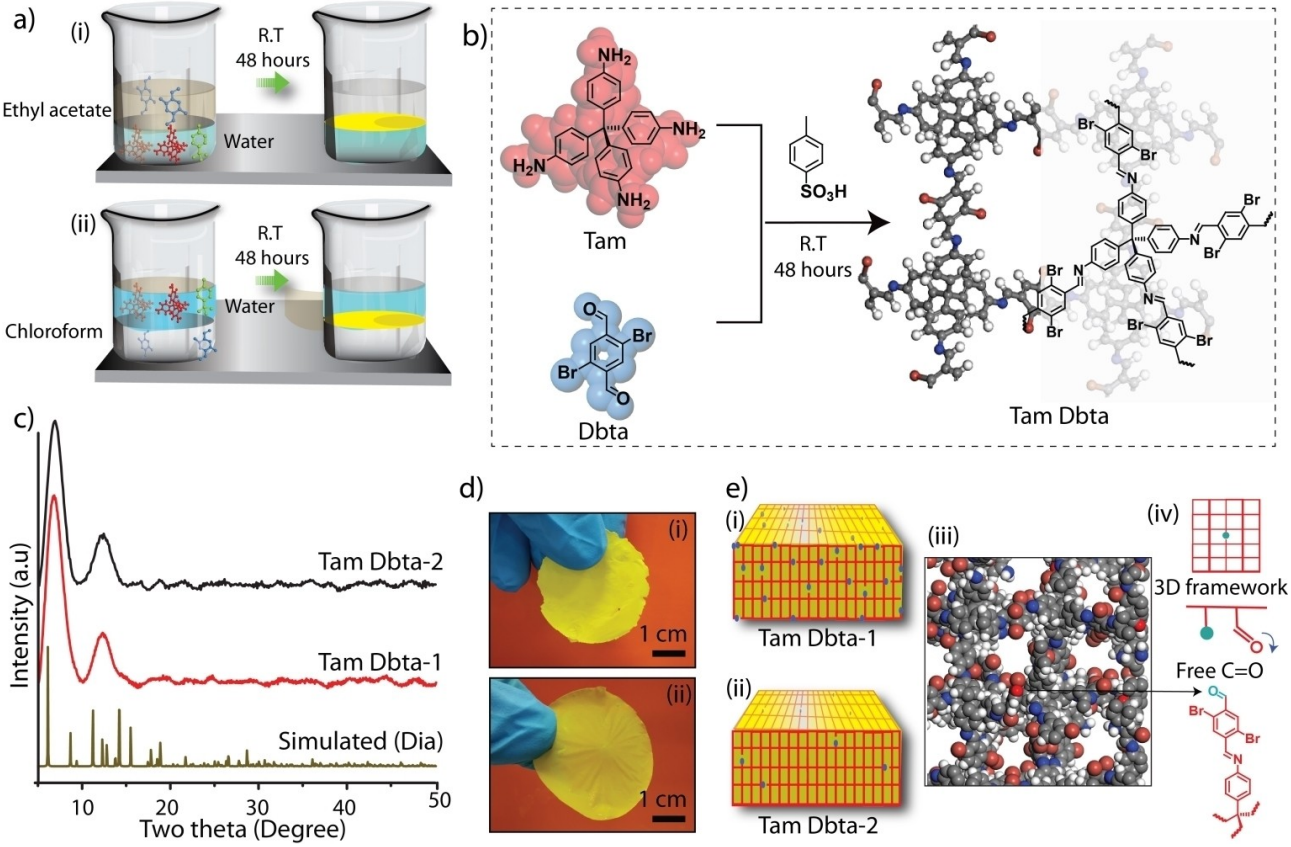

Figure 1. a) Graphical representations of the interfacial synthesis of Tam Dbta-1 and Tam Dbta-2. b) The scheme of reaction and 3D structural representation. c) The PXRD profiles of Tam Dbta-1 and Tam Dbta-2 in comparison with the simulated profile (dia-c-5). d) The digital photographs of mechanically stable, free-standing i) Tam Dbta-1 and ii) Tam Dbta-2 membranes. e) i, ii) The graphical representation of defects distributions in the frameworks. iii) Free aldehyde oxygen atoms in a representative DFT model, and iv) schematic representation of free aldehydes in 3D framework.

N-dimethylacetamide, acetone, and chloroform. Both membranes exhibit self-standing features without any further supports (Figure 1d and Figures S1–S3). The Tam Dbta-1 membrane displays a bright pale yellow colour, whereas Tam Dbta-2 has a faded dark yellowish appearance. We have also synthesized Tam Dbta (powder) through the solvothermal method for comparing the physicochemical properties with the membranes. (Synthetic details of all materials are included in Section 2, Figures S1–S6).

The atomic-level periodicity of both COF membranes was analyzed by powder X-ray diffraction (Figure 1c, and Figures S7–S11). The semi-crystalline features of the Tam Dbta-1 and Tam Dbta-2 are evident from the PXRD profiles, which display two peaks at the 2θ position of ≈6.6°, and ≈12.3°. The major peaks of the experimental PXRD patterns of both COFs match with the simulated diamond topology model (**dia-C5**). The poly-crystalline patterns of the COFs could be due to the nano-level limited growth of the 3D frameworks. The large size of –Br atoms (1.85 Å) in the C_2 linker could induce steric hindrance in the framework, which obstructs the crystalline growth into the large domains. Moreover, the absence of any monomer crystalline peaks indicates the purity of the membranes.

The disappearance of monomers was further concluded from the FT-IR spectra of the 3D-COF membranes. The absence of amine (N–H) vibration bands at 3150 cm^{-1} in the IR spectra of the membranes (Figures S12, S13) indicates the complete tetratopic imine condensation on Tam moieties. In addition, both COF membranes exhibit imine (C=N) stretching vibration at 1619 cm^{-1}. Notably, Tam Dbta-1 exhibits an intense aldehyde (C=O) stretching peak at 1696 cm^{-1}, whereas Tam Dbta-2 shows only a weak intensity aldehyde peak at 1696 cm^{-1} (Figure 2c and Figures S12, S13). It signifies organic solvents of biphase interfacial reaction control the extension of chemical bonding in Tam Dbta-1 and 2 membranes. The strong intensity of C=O peak in Tam Dbta-1 indicates the broken frameworks at diatopic C_2 moieties. Whereas, the weak intensity of C=O peak in Tam Dbta-2 signifies its less fragmentation. Again, the solvothermally synthesized Tam Dbta (powder) showed a weak intensity of C=O indicates similar bonding characteristics like less fragmented Tam Dbta-2 (Figures S14, S15).

In order to test the generality of the strategy, the membranes containing terephthaldehyde units (Ta; a bromine-free C_2 linker analogue of Dbta) were fabricated via similar interfacial synthesis (Tam Ta-1 and Tam Ta-2). Interestingly, we have observed a similar solvent-induced fragmentation effect: Tam Ta-1 (ethylacetate/water) showed a higher level of fragmentation than Tam Ta-2 (chloroform/water). Such observations are confirmed by FT-IR analysis where Tam Ta-1 showed a strong C=O peak at 1693 cm^{-1}, whereas only a weak and merged peak was observed for Tam Ta-2 (Figure S16).

The chemical environment at the atomic level of 3D-COF membranes was investigated by ^{13}C solid-state CP-MAS NMR spectroscopic analysis (Figure 2a, b and S21). Tam Dbta-1 and Tam Dbta-2 exhibit the imine carbon peaks at 154 ppm. Notably, we observed the residual aldehyde carbonyl (C=O) carbon of Tam Dbta-1 resonance at

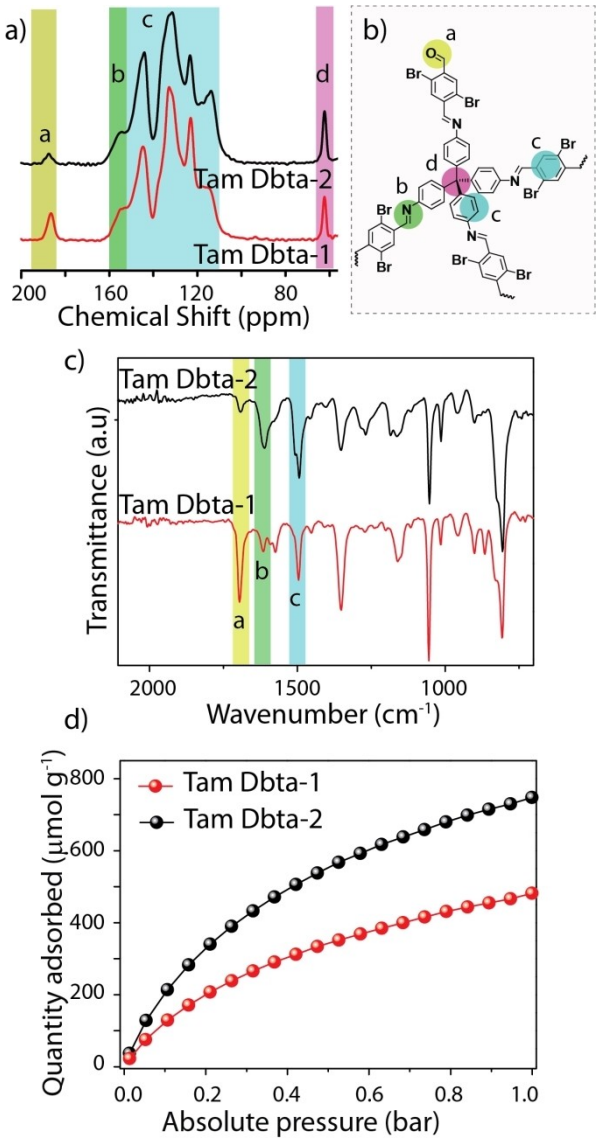

Figure 2. a) Solid-state ^{13}C-CP MAS NMR of Tam Dbta-1 and Tam Dbta-2 highlighting the difference in intensity of C=O. b) Chem-Draw image of Tam Dbta highlighting the representative atoms (coloured and labelled) for both NMR and FT-IR. c) FT-IR profiles of Tam Dbta-1 and Tam Dbta-2 show the difference in intensity of C=O and C=N bonds. d) CO_2 adsorption isotherm at 273 K (482 and 748 μmol g^{-1} for Tam Dbta-1 and Tam Dbta-2 respectively).

186.4 ppm, whereas it appeared at the chemical shift of 187.3 ppm for Tam Dbta-2. This downfield chemical shift could be due to the relatively large conjugation of Tam Dbta-2 compared to Tam Dbta-1. Moreover, the ^{13}C NMR relative peak area ratio of residual aldehyde carbon to the tetrahedral carbon in Tam Dbta-1 is ≈1 (C=O):1 (sp^3 C). However, the same relative peak area ratio in Tam Dbta-2 is ≈0.1 (C=O):1 (sp^3 C). The presence of a higher number of carbonyl moieties in Tam Dbta-1 indicates the abundance of fragmentation in the membrane (Figure 1e and Figures S22, S23).

Furthermore, to confirm the effect of solvents on the framework fragmentation, the interfacial synthesis was

carried out by using a mixture of ethylacetate and chloroform as the organic phase (30 % of ethyl acetate in 70 % of chloroform) instead of using them individually. The obtained membranes showed FT-IR spectrum with an increase in the intensity of the unreacted C=O groups (at 1696 cm^{-1}) in the framework compared to the membrane synthesized in the 100 % chloroform phase (Figure S17). This experimental analysis signifies the role of ethylacetate in the fragmentation of COF membranes. To test the role of monomer stoichiometry, two equivalence of Tam was reacted with Dbta (to provide a higher number of reactive amine groups) in ethylacetate: water interface (Figure S18). However, the IR spectra of the obtained membrane showed a sharp C=O peak at 1696 cm^{-1}, which indicates the fragmentation process irrespective of the stoichiometry. Again, the mechanism of the formation of 3D-COF membranes was investigated by time-controlled (5, 12, 24, and 48 hours) ex situ FT-IR analysis. The spectra of Tam Dbta-1 after 5 hours of reaction showed the C=N and C=O peaks with almost equal intensity (Figures S19, S20). Meanwhile, as time progresses, the intensity of C=O peak becomes more substantial compared to C=N peak. However, the Tam Dbta-2 displayed only a C=N stretching vibration at 1619 cm^{-1} after 5 hours of reaction. A very weak stretching peak of C=O (1696 cm^{-1}) was observed after 12 hours of reaction time. The mechanism suggests the augmentation of the framework fragmentation during the course of membrane formation. Herein, the discontinuity in the imine network could be due to solvation effects and reduction of pH via the reversible chemical Schiff base reaction: i) The plausible ethyl acetate hydrolysis into acetic acid at the interface of aqueous and organic layers lowers the pH and may reduce further extensions of the framework.[8] ii) Moreover, the less solubility of Dbta in ethylacetate compared to chloroform may affect the reversibility of the reaction which can further result in discontinued C=N formation from the aldehyde units in the framework.

Notably, both Tam Dbta-1 and Tam Dbta-2 COFs maintained their thermal stability up to 400 °C with a negligible loss of mass at inert conditions (Figures S24–S26). Furthermore, the porosity of these membranes was characterized by the CO_2 adsorption isotherm analysis at 273 and 298 K (Figure 2d and Figures S27–S29). Tam Dbta-2 adsorbed 748 and 439 μmol g^{-1} at 273 K and 298 K, respectively, at 1 bar. In contrast, the relatively lower CO_2 adsorption in Tam Dbta-1 (482 and 278 μmol g^{-1} at 273 K and 298 K, respectively, at 1 bar) could be because of the existence of a higher level of fragmentations with less ordered pores. The Horvath-Kawazoe pore size distribution (from Argon adsorption at 77 K) suggested the micropores of Tam Dbat-1 and Tam Dbta-2 mostly concentrated in the range of 1.1–1.3 nm (Figures S30, S31). Moreover, the dispersive micropore volume distribution of Tam Dbta-1 could be due to the presence of defects in the framework.

Transmission electron micrographs showed sheet-like nanoscale structures of Tam Dbta-1 and Tam Dbta-2 (Figure 3c and Figures S32, S33). The 3D COF membranes were further subjected to scanning electron microscopic analysis to understand their morphology in detail (Figure 3a, b and Figures S34–S40). The Tam Dbta-1 exhibits hierarchical self-assembly of 3D-COF crystallites. A uniform distribution of hollow supersphere assembly was observed on the surface of Tam Dbta-1, which was projected towards the water layer in the interfacial reaction. These hollow superspheres (diameter ≈5 to 15 μm) consist of ordered small COF microspheres (diameter ≈1.2 to 1.6 μm). The self-assembly of these COF microspheres into super spheres could be due to the weak non-covalent interactions among the COF crystallites. Moreover, the superspheres were visible as outright and partially formed spherical structures. On the other hand, the surface of Tam Dbta-1 towards ethyl acetate is evenly distributed with finger-like elongated structures (size ≈2 to 4 μm). The hierarchical morphology also consists of a thin-film (thickness of ≈1.5 μm) at the interface of superspheres and finger-like structures. The time-controlled mechanism study suggested an initial formation of the thin film at the interface of the solvent system with non-uniform distribution of individual nanospheres. As the reaction progresses, the concentration of spheres on the surface increases, and they are self-assembled into hollow superspheres (Figure S36). Notably, the hierarchical morphology of Tam Dbta-2 is different from the Tam Dbta-1. The surface projected to the water layer exhibits the aggregated self-assembled COF microspheres with sizes ≈1 to 3 μm. The shiny surface of Tam Dbta-2 displays a smooth planar morphology. Both 3D-COF membranes are continuous and devoid of any internal cracks or micro-defects. The non-contact mode AFM analysis showed the continuous "up and down" height profile of Tam Dbta-1 surface compared to a relatively flat surface of Tam Dbta-2. The 2D and 3D images signify the surface roughness originated from finger-like structures (height of ≈0.6 to 1 μm) of the Tam Dbta-1 membrane. In contrast, a planar surface was observed for Tam Dbta-2 with height increment ranges from 60 to 80 nm (Figure 3d and Figures S41, S42).

The interfacial synthesis of 3D-COF membranes offers self-standing membranes with a thickness of ≈10 to 20 μm (size of 3 cm to 8 cm) (Figure S2). Both membranes are mechanically susceptible to twisting and bending (Figure S3). The microtest tensile strength analysis revealed the elongation capacity for Tam Dbta-2 (4.4 % of initial length) is higher than Tam Dbta-1 (2.8 % of initial length) (Figure S43). Notably, the structural integrity of Tam Dbta-2 membrane was maintained for 5 minutes even after the continuous ultrasonication in chloroform. However, Tam Dbta-1 was dispersed in chloroform within 5 minutes of ultrasonication. The less mechanical strength of Tam Dbta-1 compared to Tam Dbta-2 could be due to the presence of fragmentation originated large number of defects. The intact PXRD and IR profiles suggest the maintenance of chemical stability of Tam Dbta-1 and 2 at pH = 1 for 24 hours (Figures S44, S45).

It is well known that the presence of the halogen bond can increase the hydrophobicity or lipophilicity of the material.[9] In this aspect, the enhanced hydrophobicity of Tam Dbta-1 could be related to the following reasons: 1) the presence of exposed bromine atoms on the membrane surface and 2) possible halogen bonds between bromines

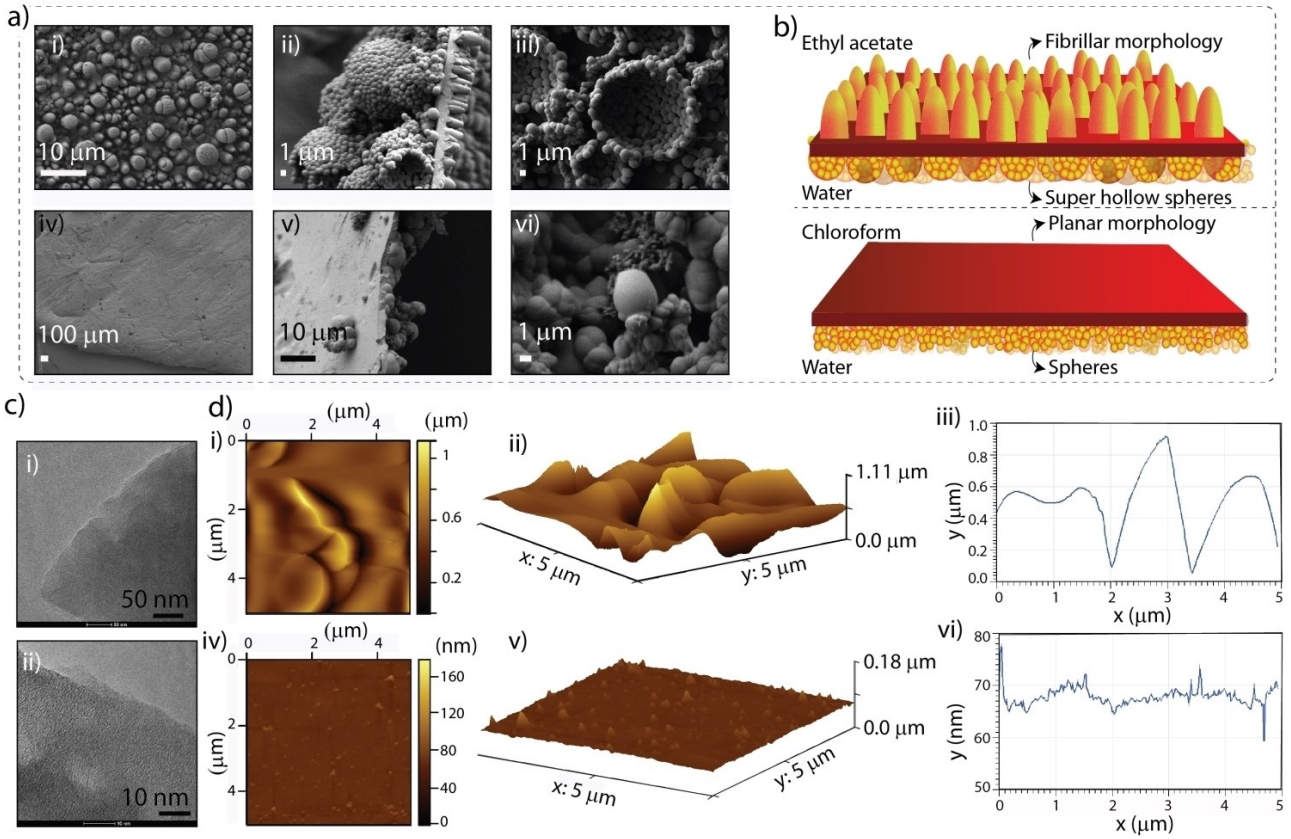

Figure 3. a) i–iii) SEM images of Tam Dbta-1 showing finger-like and super-spherical morphologies; iv–vi) SEM images of Tam Dbta-2 showing planar and spherical morphologies. b) Graphical representation of Tam Dbta-1 and Tam Dbta-2 2D sheetswith surface variations. c) TEM image of i) Tam Dbta-1 and ii) Tam Dbta-2. d) i–iii) 2D; 3D AFM images; and AFM height profile of Tam Dbta-1 and iv–vi) 2D; 3D AFM images; and AFM height profile of Tam Dbta-2.

and unreacted aldehyde oxygens in the fragments.[10] The fragmented Tam Dbta-1 leaves several exposed bromines and free aldehyde oxygens in the framework (Figure S46). A weak binding energy ($-55\,kJ\,mol^{-1}$) was found in DFT calculation when water only interacted with bromine in a molecular fragment (Figures S47,S48). Moreover, the bromine atoms in the conjugated framework are naturally electrophilic that can drive the halogen bond formation ($\approx$2.96 Å) with nucleophilic aldehyde oxygen (Br–O) (Figure S49). The strength of the halogen bond is weaker in the case of the halogen bond involving imine nitrogen (Br–N) because of the relatively lower nucleophilicity of nitrogen atoms in the framework. The nucleophilicity gradient in Tam Dbta was evident from the electrostatic potential mapping (Figure 4b and Figure S50). Considering this, we believe that the strength of the halogen bond is higher for fragmented Tam Dbta-1 compared to Tam Dbta-2. Moreover, the DFT calculations suggest that the water interaction is favourable when it sits between the COF layers, which is higher in the case of Tam Dbta-2 due to the extended network. As a result, the membrane surface of Tam Dbta-1 repels water molecules and is easily wet by oil molecules. The water contact angle measurement revealed a good hydrophobicity of Tam Dbta-1 (142°) compared to Tam Dbta-2 (60°) (Figure 4a and Figure S51). Notably, the pellet of Tam Dbta (powder) showed a very low water contact angle (<15°), which signifies the effect of fragmentation to improve the hydrophobicity (Figures S52,S53). Also, the relatively small water contact angle (72°) of bromine-free Tam Ta-1 membrane indicates the importance of bromine atoms to enhance the hydrophobicity in a fragmented membrane (Figures S54,S55).

In this regard, the flux of organic solvents through Tam Dbta-1 membranes was measured to understand the nature of interactions and transport of various polar and non-polar molecules through the membrane. The gravity-driven flux directly through the 3D-COF membranes was measured in a swinny filter apparatus (Figure 4c and d). Notably, both non-polar and polar solvents such as pentane, hexane, chloroform, and dichloromethane showed a high flux of $3490\,L\,m^{-2}\,h^{-1}$, $3126\,L\,m^{-2}\,h^{-1}$, $3293\,L\,m^{-2}\,h^{-1}$, and $3877\,L\,m^{-2}\,h^{-1}$, respectively. However, Tam Dbta-1 displayed poor flux for ethyl acetate ($131\,L\,m^{-2}\,h^{-1}$) and ethanol ($340\,L\,m^{-2}\,h^{-1}$) solvents. The flux of pentane ($2299\,L\,m^{-2}\,h^{-1}$) and hexane ($2063\,L\,m^{-2}\,h^{-1}$) through Tam Dbta-2 membrane was less than Tam Dbta-1. Conversely, Tam Dbta-2 showed a higher flux for both ethyl acetate ($817\,L\,m^{-2}\,h^{-1}$) and ethanol ($629\,L\,m^{-2}\,h^{-1}$) solvents (Figure 5a and b). It is important to note that Tam Dbta-1 strongly repelled water molecules from the surface, and

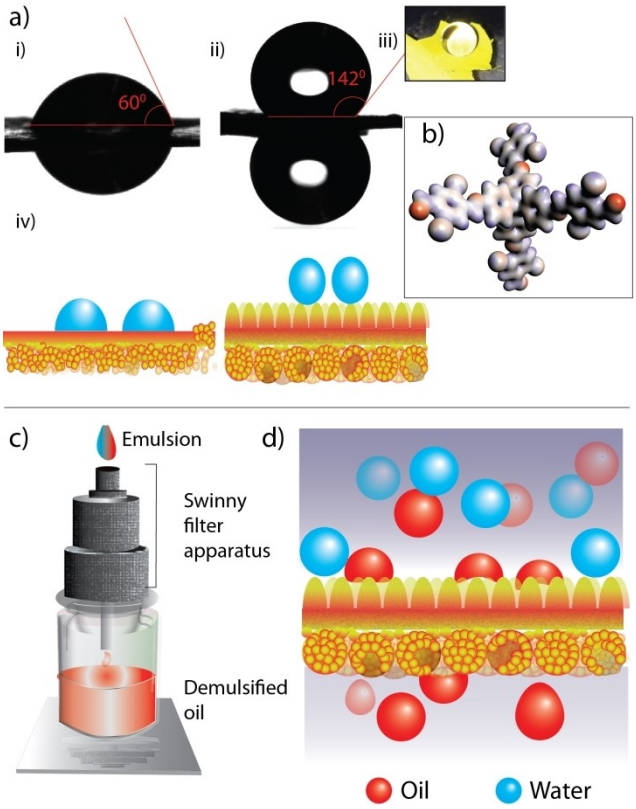

Figure 4. a) Water contact angle of i) Tam Dbta-2 and ii) Tam Dbta-1, and iii) digital photograph of water drop on Tam Dbta-1 membrane. b) Electrostatic potential mapping of the molecular fragment of Tam Dbta-1. c) Graphical representation of water–oil separation.

hence neither mass transport nor wetting of membrane was observed. On the other hand, though the water molecules could wet the Tam Dbta-2 membrane surface, the observed flux was very low ($<50\ L\,m^{-2}\,h^{-1}$).

The hydrophobicity of the Tam Dbta-1 was further explored for the effective demulsification of water–oil emulsion. The energy-efficient membrane-based oil–water separation has attracted serious research attention because of the difficulties to separate microdroplets of water from the oil phase. Water contamination in the oil phase creates several issues in oil-based industries and even in automobile systems.[11] Generally, the oil demulsification membrane should be hydrophobic to avoid the infiltration of water molecules into the membrane pores. Otherwise, it may cause the retardation of the separation flux of oil molecules.[12] Three different emulsion ratios (0.25 %, 0.5 %, and 1 % of water in oil) were investigated for the demulsification analysis. The optical microscopic images of emulsions and demulsified filtrate showed the complete removal of water microdroplets from the mixture (Figures 5c,e,f and S56). The gravity-driven demulsification flux was decreased with increasing the percentage of water (0.25 %–1536 $L\,m^{-2}\,h^{-1}$, 0.5 %–1066 $L\,m^{-2}\,h^{-1}$, 1 %–936 $L\,m^{-2}\,h^{-1}$). To the best of our knowledge, free-standing 3D-COF membranes were not reported for oil–water or any separation applications. We have demonstrated the state-of-the-art-of material in oil–water separation in Table S1. The presence of water molecules deposited on the membrane surface decreases the membrane's effective contact area and subsequently reduces the flux of hexane molecules through the membrane. The demulsified water droplets were completely deposited on the membrane surface, and then simply removed by a dropper (Figures S57, S58). However, the wetting of Tam

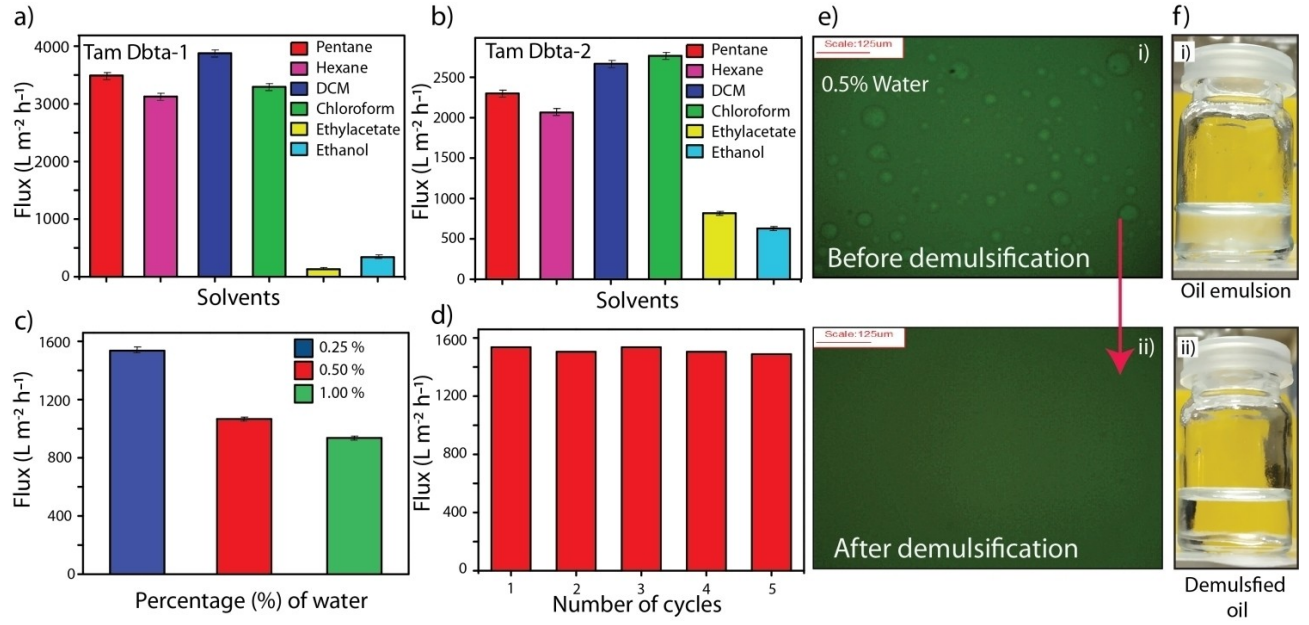

Figure 5. a) Solvent flux analysis of Tam Dbta-1 showing high flux for non-polar solvents. b) Solvent flux analysis of Tam Dbta-2. c) Oil–water demulsification flux of Tam Dbta-1. d) Recyclability analysis of oil–water demulsification by using Tam Dbta-1. e) The optical microscopic analysis of oil–water mixture i) before and ii) after demulsification. f) The digital photographs of i) oil–water emulsion and ii) demulsified oil.

Dbta-2 by water molecules (0.25 %) decreases the flux of demulsified filtrate ($450\,L\,m^{-2}\,h^{-1}$). Meanwhile, oil–water separation through the binder-free pellet (thickness $\approx 50\,\mu m$) of Tam Dbta (powder) results in severe damages to the membrane during wetting plausibly because of poor mechanical integrity. The demulsification flux of Tam Dbta-1 membrane at pH ranges from 1 to 5 (0.25 % water in oil) was noted with well maintenance of the flux ≈ 1505–$1554\,L\,m^{-2}\,h^{-1}$ (Figure S59). Moreover, the FT-IR spectra of Tam Dbta-1 showed the chemical intactness of the framework after the separation at pH = 1 (Figure S60). Furthermore, the recyclability of Tam Dbta-1 was tested for five cycles of demulsification. The membrane was dried after each separation cycle and a sustainable flux ($\approx 1500\,L\,m^{-2}\,h^{-1}$) of hexane molecules was observed (Figure 5d). The result signifies the high stability of the membrane against fouling. To examine the continuous demulsification property of Tam Dbta-1 membrane, we have performed the recyclability tests without drying the membrane. The continuous five cycles showed retardation of flux from 1536 to $1150\,L\,m^{-2}\,h^{-1}$ due to the prolonged deposition of water molecules on the membrane surface (Figure S61). The characteristic peaks in PXRD and IR of recycled membrane indicate well-maintained crystal and chemical structure of Tam Dbta-1 (Figures S62, S63). Meanwhile, the SEM images of recycled Tam Dbta-1 showed partially broken super sphere morphology, implying weak interactions among connected spheres (Figure S64).

Conclusion

We demonstrated a solvent-influenced fragmentation of 3D-COF for switching functional properties of membranes. The organic solvent plays a critical role in the PTSA-mediated imine condensation in the interfacial reaction for controlling the network formation and extent of defects. The observed fragmentation induced an extra hydrophobicity in the 3D-COF membrane via exposed halogen atoms at the defect sites. The hydrophobic 3D-COF membrane was successfully applied for the oil recovery from the oil–water emulsion. We believe that the in situ control of framework growth and functional regulation could be a potential strategy to fabricate various functional 3D-COF membranes for advanced-level applications.

Acknowledgements

D.S. and A.K.M. acknowledge Khalifa University Abu Dhabi for its generous support of this research. D.S. acknowledges the financial support from Khalifa University faculty startup grant (FSU-2020). D.S, A.A.K. and K.P. acknowledge support under RCII-2018-024. M.A.A. thanks the materials chemistry consortium for computational resources on YOUNG (EP/P020194). S.V. and M.B. acknowledge the support from NYUAD core technology platform where the solid state NMR experiments were carried out.

Conflict of Interest

The authors declare no conflict of interest.

Data Availability Statement

The data that support the findings of this study are available in the supplementary material of this article.

Keywords: Covalent Organic Framework · Halogen Bond · Hydrophobicity · Membranes · Oil–Water Separation

[1] a) C. S. Diercks, O. M. Yaghi, *Science* **2017**, *355*, eaal1585; b) A. P. Cote, A. I. Benin, N. W. Ockwig, M. O'Keeffe, A. J. Matzger, O. M. Yaghi, *Science* **2005**, *310*, 1166; c) S. Kandambeth, A. Mallick, B. Lukose, M. V. Mane, T. Heine, R. Banerjee, *J. Am. Chem. Soc.* **2012**, *134*, 19524–19527; d) C. R. DeBlase, K. E. Silberstein, T. T. Truong, H. D. Abruna, W. R. Dichtel, *J. Am. Chem. Soc.* **2013**, *135*, 16821–16824; e) S. Y. Ding, W. Wang, *Chem. Soc. Rev.* **2013**, *42*, 548–568; f) A. K. Mohammed, D. Shetty, *Environ. Sci.: Water Res. Technol.* **2021**, *7*, 1895–1927; g) S. B. Alahakoon, C. M. Thompson, A. X. Nguyen, G. Occhialini, G. T. McCandlessa, R. A. Smaldone, *Chem. Commun.* **2016**, *52*, 2843–2845; h) M. Matsumoto, L. Valentino, G. M. Stiehl, H. B. Balch, A. R. Corcos, F. Wang, D. C. Ralph, B. J. Mariñas, W. R. Dichtel, *Chem* **2018**, *4*, 308–317; i) L. Chen, J. Du, W. Zhou, H. Shen, L. Tan, C. Zhou, L. Dong, *Chem. Asian J.* **2020**, *15*, 3421–3427.

[2] a) S. Kandambeth, B. P. Biswal, H. D. Chaudhari, K. C. Rout, H. S. Kunjattu, S. Mitra, S. Karak, A. Das, R. Mukherjee, U. K. Kharul, R. Banerjee, *Adv. Mater.* **2017**, *29*, 1603945; b) C. Li, J. Yang, P. Pachfule, S. Li, M.-Y. Ye, J. Schmidt, A. Thomas, *Nat. Commun.* **2020**, *11*, 4712; c) A. Khayum M, V. Vijayakumar, S. Karak, S. Kandambeth, M. Bhadra, K. Suresh, N. Acharambath, S. Kurungot, R. Banerjee, *ACS Appl. Mater. Interfaces* **2018**, *10*, 28139–28146; d) Z. Wang, Q. Yu, Y. Huang, H. An, Y. Zhao, Y. Feng, X. Li, X. Shi, J. Liang, F. Pan, P. Cheng, Y. Chen, S. Ma, Z. Zhang, *ACS Cent. Sci.* **2019**, *5*, 1352–1359; e) K. Dey, M. Pal, K. C. Rout, H. S. Kunjattu, A. Das, R. Mukherjee, U. K. Kharul, R. Banerjee, *J. Am. Chem. Soc.* **2017**, *139*, 13083–13091.

[3] a) F. J. Uribe-Romo, J. R. Hunt, H. Furukawa, C. Klock, M. O'Keeffe, O. M. Yaghi, *J. Am. Chem. Soc.* **2009**, *131*, 4570–4571; b) S. Wang, X.-X. Li, L. Da, Y. Wang, Z. Xiang, W. Wang, Y.-B. Zhang, D. Cao, *J. Am. Chem. Soc.* **2021**, *143*, 15562–15566; c) Z. Li, H. Li, X. Guan, J. Tang, Y. Yusran, Z. Li, M. Xue, Q. Fang, Y. Yan, V. Valtchev, S. Qiu, *J. Am. Chem. Soc.* **2017**, *139*, 17771–17774; d) X. Guan, F. Chen, Q. Fang, S. Qiu, *Chem. Soc. Rev.* **2020**, *49*, 1357–1384; e) Y. Ma, Y. Wang, H. Li, X. Guan, B. Li, M. Xue, Y. Yan, V. Valtchev, S. Qiu, Q. Fang, *Angew. Chem. Int. Ed.* **2020**, *59*, 19633–19638; *Angew. Chem.* **2020**, *132*, 19801–19806.

[4] a) J. M. Rotter, S. Weinberger, J. Kampmann, T. Sick, M. Shalom, T. Bein, D. D. Medina, *Chem. Mater.* **2019**, *31*, 10008–10016; b) Z. Wang, Z. Si, D. Cai, G. L. S. Li, P. Qin, *J. Membr. Sci.* **2020**, *615*, 118466; c) H. Lu, C. Wang, J. Chen, R. Ge, W. Leng, B. Dong, J. Huang, Y. Gao, *Chem. Commun.* **2015**, *51*, 15562–15565; d) Z. Zhang, N. Han, L. Tan, Y. Qian, H. Zhang, M. Wang, W. Li, Z. Cui, X. Zhang, *Langmuir* **2019**, *35*, 16545–16554; e) Y. Yang, S. Mallick, F. I. -Ruiz, C. Schäfer, X. Xing, M. Rahm, K. Börjesson, *Small* **2021**, *17*, 2103152.

[5] a) M. S. Lohse, T. Bein, *Adv. Funct. Mater.* **2018**, *28*, 1705553; b) Y. Liu, W. Li, C. Yuan, L. Jia, Y. Liu, A. Huang, Y. Cui,

Angew. Chem. Int. Ed. **2022**, *61*, e202113348; *Angew. Chem.* **2022**, *134*, e202113348.
[6] a) Y. Deng, Y. Wu, G. Chen, X. Zheng, M. Dai, C. Peng, *Chem. Eng. J.* **2021**, *405*, 127004; b) C. Su, T. Horseman, H. Cao, K. Christie, Y. Li, S. Lin, *Environ. Sci. Technol.* **2019**, *53*, 11801–11809; c) J. Liu, D. Hua, Y. Zhang, S. Japip, T.-S. Chung, *Adv. Mater.* **2018**, *30*, 1705933.
[7] S. Zhao, C. Jiang, J. Fan, S. Hong, P. Mei, R. Yao, Y. Liu, S. Zhang, H. Li, H. Zhang, C. Sun, Z. Guo, P. Shao, Y. Zhu, J. Zhang, L. Guo, Y. Ma, J. Zhang, X. Feng, F. Wang, H. Wu, B. Wang, *Nat. Mater.* **2021**, *20*, 1551–1558.
[8] a) H. A. Smith, J. H. Steele, *J. Am. Chem. Soc.* **1941**, *63*, 3466–3469; b) O. R. Pierce, G. Gorin, *J. Am. Chem. Soc.* **1953**, *75*, 1749–1750.
[9] a) G. Cavallo, P. Metrangolo, R. Milani, T. Pilati, A. Priimagi, G. Resnati, G. Terraneo, *Chem. Rev.* **2016**, *116*, 2478–2601; b) A. Priimagi, G. Cavallo, P. Metrangolo, G. Resnati, *Acc. Chem. Res.* **2013**, *46*, 2686–2695; c) G. Berger, J. Soubhyea, F. Meyer, *Polym. Chem.* **2015**, *6*, 3559.
[10] O. Bolton, K. Lee, H.-J. Kim, K. Y. Lin, J. Kim, *Nat. Chem.* **2011**, *3*, 205–210.
[11] a) M. Ge, C. Cao, J. Huang, X. Zhang, Y. Tang, X. Zhou, K. Zhang, Z. Chen, Y. Lai, *Nanoscale Horiz.* **2018**, *3*, 235–260; b) R. K. Gupta, G. J. Dunderdale, M. W. England, A. Hozumi, *J. Mater. Chem. A* **2017**, *5*, 16025–16058.
[12] a) M. Padaki, R. S. Murali, M. S. Abdullah, N. Misdan, A. Moslehyani, M. A. Kassim N Hilal, A. F. Ismail, *Desalination* **2015**, *357*, 197–207; b) J. Gao, X. Huang, H. Xue, L. Tang, R. K. Y. Li, *Chem. Eng. J.* **2017**, *326*, 443–453.

Manuscript received: January 18, 2022
Accepted manuscript online: January 23, 2022
Version of record online: February 19, 2022